Letter to the Editor

The new complex gravitational lens system HE 0230−2130[⋆]

L. Wisotzki[1], **N. Christlieb**[1], **M.C. Liu**[2,⋆⋆], **J. Maza**[3], **N.D. Morgan**[4,⋆⋆], and **P.L. Schechter**[4,⋆⋆]

[1] Universität Hamburg, Hamburger Sternwarte, Gojenbergsweg 112, D-21029 Hamburg, Germany
[2] University of California, Department of Astronomy, Berkeley, CA 94720, USA
[3] Universidad de Chile, Departamento Astronomia, Casilla 36-D, Santiago, Chile
[4] Massachusets Institute of Technology, Department of Physics, Cambridge, MA 02138, USA

Abstract. We report the discovery of the new gravitational lens system HE 0230−2130, a QSO at redshift $z = 2.162$ consisting of at least five distinct components. Three of these are clearly lensed images of the QSO, one is most likely the lensing galaxy, while for the fifth component the identity is unclear: It could be a fourth QSO image (if so, then highly reddened), or another intervening galaxy, or a superposition of the two. Differential reddening seems to be important also for the first three QSO images. The surface density of faint galaxies near the QSO appears to be enhanced by a factor of $\gtrsim 2$, indicating the presence of a distant cluster close to the line of sight.

Key words: cosmology: gravitational lensing – galaxies: quasars: general – galaxies: quasars: individual: HE 0230–2130

1. Introduction

The study of gravitational lenses has become a powerful tool to address several distinct cosmological and astrophysical questions. These include the distribution of dark matter in galaxies (Keeton et al. 1998), studying dust extinction at redshift $z \gg 0$ (Nadeau et al. 1991; Jean & Surdej 1998), and determining the Hubble parameter H_0 from measurements of light travel time delay between different lines of sight (Refsdal 1964). The appeal of this method lies in its complete independence of the traditional cosmic distance ladder, yielding distances for high-redshift objects in a single leap.

The uncertainties of H_0 estimation are mainly limited by ambiguities in modelling the deflector mass distribution, since all relevant *measurement* errors can be reduced to insignificance. While 'simple' lenses such as double QSOs do not strongly con-

strain the deflector model, multiple systems such as quadruply imaged QSOs provide many additional constraints, allowing e.g. to independently test the assumed mass distribution models (cf. Saha & Williams 1997). A problem with quadruple systems, however, can be excessive symmetry leading to time delays which are short compared to intrinsic radio and optical variability timescales, as in the famous 'Einstein Cross' 2237+030 or in the 'Clover Leaf' H 1413+117.

In this paper we present the discovery of the new multiple QSO HE 0230−2130. The object was originally identified as a high-probability QSO candidate in the course of the Hamburg/ESO survey (Wisotzki et al. 1996) and subsequently observed as part of a large imaging search for lensed QSOs. The coordinates of this object are R.A. = 02$^{\mathrm{h}}$ 32$^{\mathrm{m}}$ 33$^{\mathrm{s}}$1, Dec = −21° 17′ 26″ (J2000.0), as measured in the *Digitized Sky Survey*.

2. Observations

Imaging data were obtained at the CTIO 1.5 m on 13 November 1998, in Johnson B and R, and Cousins I. In each band, three images were taken of 5 min exposure time each. The seeing was somewhat variable: 1″ in B, 1″.1 in R, and 0″.8 in I. Pixel size was 0″.24. Small sections of these images are reproduced in Fig. 1, revealing the multiple structure of the QSO already at first glance. Two almost merging images (A1 and A2; see Fig. 2) of nearly equal brightness dominate the total magnitudes. Another discrete component, B, is clearly apparent with roughly similar colours. Components C and D are much less prominent, and in fact appear as two distinct sources rather than just one only in I.

On the same night, near-infrared (K_s band, 2.0–2.3 μm) images were taken at the CTIO 4 m telescope with the CIRIM imager. Total exposure time was 18 min under 0″.9 seeing. The pixel size of the raw data was 0″.42, but the single exposures were combined on a $2\times$ finer grid; the resulting image is also shown in Fig. 1. The centrally located component D is now almost as bright as A1 and A2 and unambiguously separated from
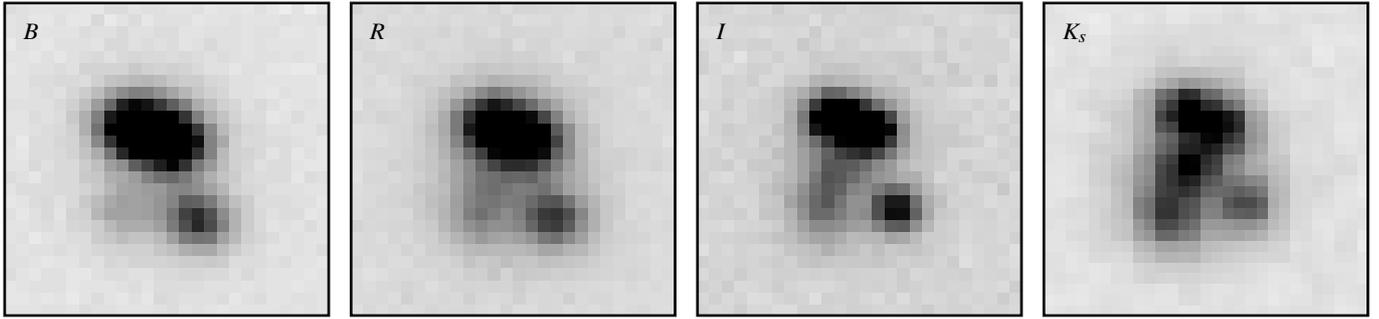
Fig. 1. *BRIK* band images of the multiple QSO system. Each subimage measures $6'' \times 6''$; north is up, east is to the left.

C. A quantitative analysis of the astrometric and photometric properties is given in the next section.

At the time of these observations, HE 0230−2130 had been a mere QSO candidate based on a digital objective prism spectrum, with an estimated redshift of $z \simeq 2.165$. Although we had little doubt about its QSO nature, confirmation was clearly needed. We obtained a first low-resolution spectrum on 23 November 1998 with the ESO/Danish 1.5 m telescope equipped with DFOSC. A slit of $2''$ positioned East-West gave a spectral resolution of $\sim 20\,\text{Å}$ FWHM. The rather poor seeing of $1''8$ inhibited all attempts to separate different components; and the spectrum, displayed in Fig. 3, represents more or less the superposition of all components. It shows a typical QSO with $z = 2.162$, as measured from the centroid of the Mg II emission line.

An attempt to obtain individual spectra of different components was made at the ESO 3.5 m NTT on 10 December 1998, using the red arm of EMMI with grism #3 and a $1''$ slit, at $8\,\text{Å}$ resolution. Only one spectrum could be taken, with the slit oriented North-South crossing A2 and B. At a seeing of $0''5$, the components were well separated, showing two QSO spectra at the same redshifts. Unfortunately, the spectrum of B suffers from substantial slit losses: While the flux ratio A2/B is 2.3 in the red, in good agreement with the PSF photometry described below, it increases to $\gtrsim 6$ at the blue end around $4000\,\text{Å}$. To correct for these losses, the quotient spectrum was fitted with a 5th-order polynomial, and the spectrum of B was multiplied by the fit, thereby adjusting both spectra to the same global level of relative fluxes. The result is displayed in Fig. 4 and discussed below.

3. Analysis

3.1. Astrometry

To decompose the complex configuration into discrete sources, we employed the DAOPHOT II software package as implemented within ESO-MIDAS. For the optical images, a numerical composite PSF was built for each image using three bright stars at $\sim 1'$ distance to the QSO. In the K band data no bright PSF star was available within the small field of view, and a purely analytical PSF was estimated from the only two isolated stars in the field. The QSO was then modelled by the super-
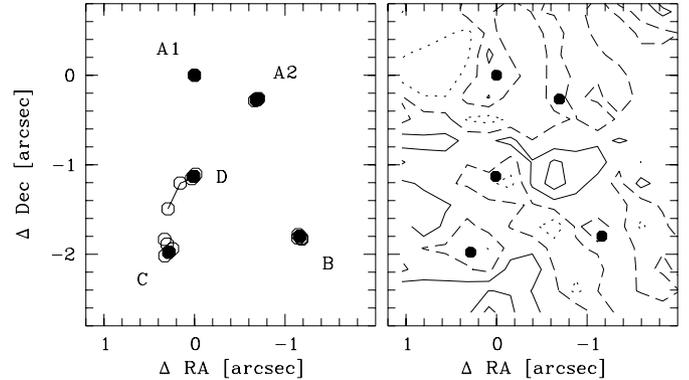

Fig. 2. *Left panel:* Adopted nomenclature and measured positions of the five components. Filled black circles give the positions from Table 1, open circles show individual measurements in the different photometric bands. *Right panel:* Contour plot of residual I band image after subtraction of five point sources. The dashed contour shows the zero level, while negative residuals are dotted, and positive residuals are surrounded by the solid contours. Contour difference is $2\times$ the photon shot noise in each pixel.

position of five point sources, with positions and PSF scaling factors simultaneously optimised (routine ALLSTAR). Fitting five components gave always a significantly better fit, in terms of residual χ^2, than with four, even in the B band image where C and D are both very faint. The fitting results are collected in Tables 1 and 2. Positions are measured relative to A1, which was arbitrarily taken as reference point.

For components A1, A2, and B, the positions measured in the four *BRIK* images are very consistent, and the scatter between the photometric bands reflects the measurement error. For C and D, image positions are consistent only between I and K; at shorter wavelengths, the fitted centroids approach each other as illustrated in Fig. 2. This could be related to different intrinsic colours of the objects, but could also be an artefact of low S/N and the somewhat poorer seeing in the shorter wavelength data.

3.2. Photometry

Differential PSF photometry of the QSO components relative to A1 was available from the ALLSTAR analysis (Table 2).
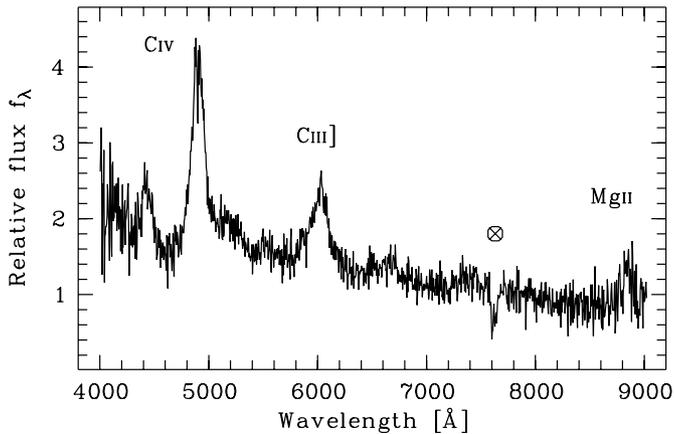
Fig. 3. Spectrum of HE 0230−2130 taken with the ESO/Danish 1.5 m telescope at poor seeing; the spectrum is the sum of all components.

Table 1. Differential astrometry for HE 0230−2130, based on the I and K band images.

Component	$\Delta\alpha$ [arcsec]	$\Delta\delta$ [arcsec]
A1	0.00	0.00
A2	-0.68 ± 0.01	-0.27 ± 0.01
B	-1.17 ± 0.02	-1.80 ± 0.02
C	0.28 ± 0.04	-1.98 ± 0.04
D	0.01 ± 0.02	-1.13 ± 0.03

Table 2. Differential photometry of HE 0230−2130. The first row gives the total magnitude from aperture photometry, all other entries were computed relative to these values.

Component	B	R	I	K
Total	18.20 ± 0.01	17.66 ± 0.01	17.18 ± 0.01	14.96 ± 0.02
A1	19.27 ± 0.02	18.83 ± 0.02	18.49 ± 0.02	16.54 ± 0.04
A2	19.27 ± 0.02	18.89 ± 0.02	18.43 ± 0.02	16.65 ± 0.04
B	20.06 ± 0.02	19.45 ± 0.02	19.00 ± 0.02	16.95 ± 0.04
C	21.87 ± 0.08	20.42 ± 0.04	19.74 ± 0.05	16.80 ± 0.04
D	22.02 ± 0.24	20.62 ± 0.05	19.63 ± 0.04	16.65 ± 0.05

Table 3. Colours of the components in HE 0230−2130, based on the PSF magnitudes from Table 2.

Component	$B - R$	$R - I$	$I - K$
A1	0.44	0.34	1.95
A2	0.38	0.45	1.78
B	0.62	0.45	2.05
C	1.45	0.68	2.94
D	1.40	0.98	2.98

Flux calibration was established separately using simple aperture photometry (aperture diameter was $9''\!.6$ for *BRI* and $7''\!.5$ for K_s). Standard stars from the RU 149 field (Landolt 1992) served to obtain colour terms and photometric zeropoints in the optical, while SJ 9106 (Persson et al. 1998) was used for the NIR photometry.

The total magnitudes thus measured are listed in the first line of Table 2, with uncertainty estimates as given in the DAOPHOT output. We have also determined aperture *BRI* magnitudes for 14 nearby stars in the field that may be useful to serve as reference stars in future monitoring. A list with these measurements is available on request.[1]

The relative photometry confirms that A1, A2, and B have very similar optical-NIR colours although B appears slightly redder than A1 and A2. C and D are much redder, on the other hand, so neither can correspond to a single unobscured fourth QSO image. Because of the apparent positional shift between the bands, we computed a second model with fixed positions imposed from the I band image, fitting only the PSF scaling factors. The resulting colours are slightly bluer for components B and C, and even much redder for D. However, inspection of the PSF-subtracted images indicated that the fit quality of these restricted models was much poorer, leaving residuals significant on the 2–3σ level.

3.3. Spectroscopic properties

While in double QSOs there is always the possibility that a true binary system is being observed, a configuration like that seen in HE 0230−2130 is almost certainly best explained as a lensed system, even without spectroscopic evidence. Although we do not yet have spectra of all components, the available data allow nevertheless to confirm the lens hypothesis beyond all reasonable doubt:

(1) The total spectrum (Fig. 3) contains no trace of absorption features that would be expected if A1 was a star or a galaxy. We conclude that A1 and A2 have most probably very similar spectra, given the broad-band colours.

(2) A2 and B have both very similar QSO spectra, apart from the slit loss effects. Fig. 4 shows that the emission line centroids agree within the measurement accuracy, the line widths are equal, and also the strong 'associated' ($z_{\rm abs} \simeq z_{\rm em}$) C IV absorption system is clearly present in both components.

A curious feature, however, are the significant residuals detected in the difference spectrum A2–B(scaled), indicating non-identical emission line profiles and/or equivalent widths. Whether this might be due to differences in intervening line absorption along the lines of sight, or due to selective continuum microlensing such as proposed in HE 1104−1805 (Wisotzki et al. 1993) remains to be explored; the current data do not permit a more detailed analysis.
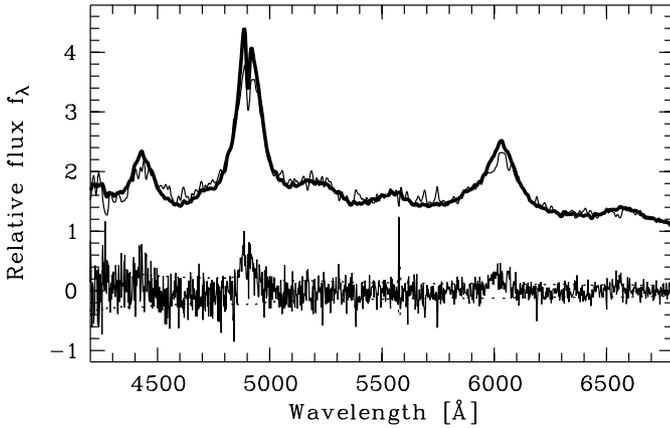
---

[1] NDM; email: ndmorgan@mit.edu

Fig. 4. Comparison between the NTT spectra of components A2 and B (slightly smoothed). The thick line shows A2, the thin line shows B after correction for slit losses (see text). Below the unsmoothed difference of both spectra is plotted together with the $\pm 1\sigma$ envelope expected from pure shot noise (dashed line).
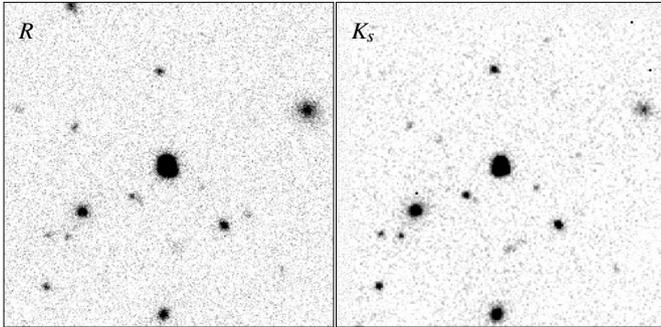

Fig. 5. R and K_s band images ($1' \times 1'$) showing the possible galaxy cluster around the QSO. The QSO is the bright object in the centre; north is up, east is to the left.

3.4. Nearby galaxies

Visual inspection of the available images (see Fig. 5) shows a number of faint galaxies in the vicinity of the QSO, but most of these objects are very faint and at the limit of the present data ($R_{\rm lim} \simeq 23$, $I_{\rm lim} \simeq 22.5$, $K_{s,\rm lim} \simeq 20.5$). The surface density of faint objects around the QSO (within $\sim 30''$ radius) was found to be enhanced by a factor of 2–3 compared to the surrounding regions. As star-galaxy separation was not reliable for such faint sources, every detected object was counted, so the overdensity is a conservative estimate. However, the signal is significant only on the 2σ level, using Poisson statistics.

Most of the ~ 20 objects within $30''$ from the QSO are detected in RIK_s (and expectedly not in B). The $R-I$ and $I-K$ colours show relatively little dispersion and are consistent with galaxy colours at low to intermediate redshifts, $z \lesssim 0.6$ (cf. Fukugita et al. 1995). We conclude that there is some evidence for a cluster near the line of sight to HE 0230−2130, but that this has to be confirmed by deeper imaging and spectroscopy.

4. Discussion

Components A1, A2, and B of HE 0230−2130 have been clearly identified, by multicolour imaging and spectroscopically, as being images of one and the same QSO. The identities of components C and D have not yet been ascertained. From their locations, a reasonable guess might be that C is the expected fourth image and D the lensing galaxy. The colours of D are certainly consistent with this notion, but the case is more complicated with component C. Using only positions as constraints, simple models which take C to be the 4th image give large residuals, whereas models which fit only the positions of images A1, A2 and B are poorly constrained. Moreover, the colours colours of C are very different from the confirmed QSO components. This might indicate either heavy reddening by dust in the fourth image, or the presence of a second galaxy, or even superposition of a galaxy *plus* fourth image. Without spectroscopic information on C we presently cannot decide between these possibilities.

If C is partly or largely due to a galaxy, it is *a priori* most likely (but not granted) that C and D are at the same redshifts, forming one common deflector plane. If, on the other hand, C is formed by just the fourth quasar image, this would be one of the few known lenses with strongly differential dust extinction, and the first optically selected one. Furthermore, the inferred amount of differential extinction would be $\Delta E(B-V) \simeq 0.4$, just intermediate between the very small and highly uncertain values found for most lenses and the few cases where the light path in the optical is strongly obscured (cf. Falco et al. 1999).

HE 0230−2130 is an interesting new target for photometric monitoring. It is moderately symmetric so that the time delay is probably much shorter than a year, avoiding the considerable windowing problem of observations stretching over several years. Yet, it displays enough departure from symmetry that the time delay will not be uncomfortably low. In many respects, it resembles PG 1115+080, the presently cleanest system for determination of H_0 (e.g., Schechter et al. 1997). The apparent magnitude and colour of the putative lensing galaxy suggest that its redshift is not too high, $z_l \lesssim 0.6$.

References

Falco E.E., Impey C.D., Kochanek C.S., et al., 1999, ApJ submitted, astro-ph/9901037
Fukugita M., Shimasaku K., Ichikawa T., 1995, PASP 107, 945
Jean C., Surdej J., 1998, A&A 339, 729
Keeton C.R., Kochanek C.S., Falco E.E., 1998, ApJ 509, 561
Landolt A.U., 1992, AJ 104, 340
Nadeau D., Yee H.K.C., Forrest W.J., et al., 1991, ApJ 376, 430
Persson S.E., 1998, AJ 116, 2475
Refsdal S., 1964, MNRAS 128, 295
Saha P., Williams L., 1997, MNRAS 292, 148
Schechter P.L., Bailyn C.D., Barr R., et al., 1997, ApJ 475, L85
Wisotzki L., Köhler, T., Kayser R., Reimers D., 1993, A&A 278, L15
Wisotzki L., Köhler T., Groote D., Reimers D., 1996, A&AS 115, 227